Simultaneous transfer ionization of a negative hydrogen ion by positron impact

D. Ghosh and C. Sinha
Theoretical Physics Department, Indian Association for the Cultivation of Science, Kolkata 700032, India
(Received 19 June 2003; revised manuscript received 19 September 2003; published 9 December 2003)

A model has been proposed to investigate theoretically, the simultaneous electron capture and the ejection of another electron by which a bare hydrogen ion and a positronium atom (Ps) are produced in a single collision between a positron and a negative hydrogen ion (H^-). The angular distributions of the scattered Ps atom as well as of the ejected electron are studied in the intermediate- and high-energy regimes (40–200 eV) with respect to the threshold energy for this particular transfer ionization (TI) process. The electron-electron correlation effect that mainly governs such two-electron transition processes in this energy regime has been taken into account in both the initial and final channels. The long-range Coulomb attraction between the incident positron and the negative hydrogen ion in the initial channel has also been incorporated properly. Signature of the so-called Thomas peak (a double-peak structure) predicted for charge-transfer or transfer-ionization process for heavy-particle projectiles in the high-energy regime has also been noted in the present TI process (for light projectile e^+) and could be attributed to the correlated e^+-e-e scattering mechanism. In addition, the fully differential (triple) cross sections for different kinematics reveal some structures unusual for a pure transfer or a pure ionization process which are to be verified by the future experiments.

DOI: 10.1103/PhysRevA.68.062701 PACS number(s): 34.70.+e, 34.90.+q

I. INTRODUCTION

A full understanding of the dynamics of a correlated many-body Coulomb system is still one of the major fundamental challenges in atomic collision physics. In view of the recent spectacular advances in multicoincidence techniques, it has now become possible to have the energy and angle-resolved simultaneous detection of two or three final-state electrons in a kinematically complete experiment that measures the fully differential cross sections for some two-electron transition processes in atomic system by electron/photon impact, where the many-body interactions are of prime importance. Such fully differential measurements are very much sensitive to the interelectronic correlation both in the initial and final states. Following these experiments, studies on electron-electron correlation effect in different multielectron transition processes are finding increasing attention from the theoretical physicists.

The challenge in the theoretical investigations of these processes lies in the modeling and understanding of the inherently entangled many-body Coulomb system and in the treatment of the particular difficulties associated with the infinite range of the Coulomb potentials acting between different pairs of charged particles involved in the process.

Simultaneous capture (transfer) and ionization of a two-electron (or multielectron) target, commonly known as transfer ionization (TI), is one of the aforesaid correlated processes in which the projectile captures an electron from the target while another electron of the target gets ionized simultaneously. A significant number of differential measurements (angular distributions) [1–4] exist in the literature for the simultaneous TI process of He atom by heavy-particle impact (e.g., H^+) whereas for a light projectile e^+, the experiments performed on the TI process are mainly limited to measurements of total cross sections for some noble-gas targets [5,6]. To our knowledge, the only differential measurement [7] reported so far for e^+ impact TI process is on $e^+ + Ar$ system, where one of the electrons from the outermost shell of an Ar atom is captured by the incident e^+ to form a Ps atom while another electron gets ionized in a single collision.

However for a theoretical study of such TI process, the simplest two-electron atoms (e.g., He, H^-) should be the most preferred multielectron target. For He target, the total double-ionization (DI) cross sections by e^+ impact have been measured [8] including the transfer-ionization channel in the low-energy regime where it was found that the Ps channel is strongly suppressed in the second ore gap region where TI is the only open channel for the DI process of the target atom.

The present study concerns the simultaneous transfer and ionization (TI) process in a positron–negative hydrogen ion collision, for which both the electron-capture and single-ionization probabilities are expected to be much higher than those for the neutral He target (the ionization potential of the H^- ion being very low as compared to the He atom). Thus the present work deals with the process

$$e^+ + H^- \rightarrow (e^+ e) + H^+ + e. \tag{1}$$

To our knowledge, the present work is the first theoretical attempt for the study of TI process of the H^- ion by e^+ impact. As a first step, we have considered the case when the Ps atom is formed in the ground state only, although there is a probability that the Ps may be formed in excited states as well.

The choice of negative hydrogen ion H^- as a target for such two-electron transition process is mainly dictated by the fact that the H^- ion is basically a strongly correlated system, its very existence being due to electron-electron correlation. Further, since negative hydrogen ion has some properties unlike the neutral atom (He), e.g., possessing no bound excited state below the first detachment threshold, it finds some additional importance from the experimentalists. Regarding

practical applications, dissociation of H^- ion by electron/positron impact is of much astrophysical interest, particularly because of its relevance to solar and stellar opacities [9(a)– 9(c)]. In fact, the detachment of H^- ion by electron/photon impact has been the subject of experimental and theoretical studies [10(a)–10(g)] long since, till now.

In pure single-selectron capture, besides the energy and momentum exchange between the projectile and the active electron, the transfer of energy and momentum to a third particle is also required during the courses of the collision. In nonradiative collisions, this third particle can be either the target nucleus or, for multielectron atoms, one of the electrons that is not captured.

Theoretically, a pure electron-capture process can occur due to different reaction mechanisms: (1) kinematical capture, arising due to velocity matching between the projectile and the active electron, (2) Thomas nucleus-electron, i.e., *p-n-e* scattering [11], and (3) Thomas electron-electron, i.e., *p-e-e* scattering [11], where *p* stands for the projectile. Now in the TI process, where a second electron is to be ejected, the *p-e-e* capture process takes account of this automatically in which the projectile first scatters inelastically at one of the target electrons and then in a second interaction this electron scatters at the other target electron (through the *e-e* correlation), so that finally one target electron is emitted into the target continuum while the other electron forms a bound state with the incident projectile in ground or excited states. In fact, if the energy transfer in the *e-e* collision is much larger than the binding energy of the electron in the particular atom, it leads to TI process.

On the other hand, the other two capture processes (1) and (2) must be accompanied by an additional process such as shake off by which the second electron is ejected. The transfer-ionization process can also occur due to two independent interactions (uncorrelated) between the projectile and the two target electrons in separate encounters, which is usually termed as two-step mechanism (TS2). This process (TS2) is second order in the projectile-target interaction potential since it involves two successive binary collisions and should be treated in the framework of the second Born-type theory. Different aforesaid mechanisms for the TI process are supposed to dominate in different kinematical situations; e.g., the shake off and the so-called Thomas *p-e-e* mechanism, being first order in the projectile-target interaction, are expected to dominate at high incident energy while the TS2, being second order in the interaction potential, is supposed to be more important at comparatively lower incident energy regime.

The present prescription has been formulated on the basis of correlated *p-e-e* mechanism, the signature of which has already been noted much ago in the experiments for proton—He collisions [1–4].

II. THEORY

The transition matrix element for the TI process (1) is given by

$$T_{if}=\langle \Psi_f^-(\vec{r}_1,\vec{r}_2,\vec{r}_3)|V_i|\Psi_i(\vec{r}_1,\vec{r}_2,\vec{r}_3)\rangle, \tag{2}$$

where $\vec{r}_1$, $\vec{r}_2$, and $\vec{r}_3$ are the respective coordinates of the incident positron (e^+) and the two bound electrons with respect to the target nucleus.

The total Hamiltonian in the initial channel for the e^+-H^- ion system may be written as (in atomic units)

$$H_i=H_0+\frac{(Z_t-2)}{r_1}+\frac{2}{r_1}-\frac{Z_t}{r_2}-\frac{Z_t}{r_3}-\frac{1}{r_{12}}-\frac{1}{r_{13}}+\frac{1}{r_{23}}, \tag{3a}$$

where $\vec{r}_{12}=\vec{r}_1-\vec{r}_2$, $\vec{r}_{13}=\vec{r}_1-\vec{r}_3$, $\vec{r}_{23}=\vec{r}_2-\vec{r}_3$, and Z_t being the charge of the target H^- ion ($Z_t=1$). The full kinetic-energy operator H_0 in Eq. (3a) is given by

$$H_0=-\frac{1}{2}\nabla_1^2-\frac{1}{2}\nabla_2^2-\frac{1}{2}\nabla_3^2. \tag{3b}$$

The wave function of the incident positron in the attractive Coulomb field of the H^- ion satisfies the following Schrödinger equation:

$$\left(-\frac{1}{2}\nabla_1^2+\frac{(Z_t-2)}{r_1}-\frac{k_i^2}{2}\right)\chi_i(\vec{r}_1)=0. \tag{4}$$

The solution $\chi_i(\vec{r}_1)$ of Eq. (3) is given as

$$\chi_i(\vec{r}_1)=\exp\left(\frac{\pi\alpha_i}{2}\right)\Gamma(1-i\alpha_i)\times e^{i\vec{k}_i\cdot\vec{r}_1}{}_1F_1[i\alpha_i,1;i(k_ir_1-\vec{k}_i\cdot\vec{r}_1)],$$

where $\alpha_i=-1/|\vec{k}_i|$ and $\vec{k}_i$ is the initial momentum of the incident positron.

The correlated wave function [12] $\Phi_i(\vec{r}_2,\vec{r}_3)$ of the target H^- ion is chosen as

$$\Phi_i(\vec{r}_2,\vec{r}_3)=N_i[\exp(-\lambda_a r_2-\lambda_b r_3)+\exp(-\lambda_b r_2-\lambda_a r_3)]\times[1+C_0\exp(-\lambda_c r_{23})], \tag{5}$$

with $N_i=0.218\,740\,4$, $\lambda_a=0.4651$, $\lambda_b=1.0713$, $\lambda_c=0.0562$, and $C_0=-0.8657$. The ground-state energy [12] of the H^- ion for this wave function is $E=-0.526\,001$ atomic unit (a.u.) and the corresponding electron affinity is $-0.026\,001$ a.u.

The initial-state wave function Ψ_i is the product of the wave function for the incident positron and the correlated ground-state wave function of the H^- ion, i.e.,

$$\Psi_i(\vec{r}_1,\vec{r}_2,\vec{r}_3)=\Phi_i(\vec{r}_2,\vec{r}_3)\chi_i(\vec{r}_1). \tag{6}$$

In view of Eqs. (2)–(4), the initial channel perturbation V_i in Eq. (2), which is the part of the total interaction not diagonalized in the initial state, is given by

$$V_i=\frac{2}{r_1}-\frac{1}{r_{12}}-\frac{1}{r_{13}}. \tag{7}$$

It may be noted from Eq. (7) that the perturbation V_i vanishes asypmtotically (for $r_1\to\infty, r_2, r_3$ finite).

For the construction of the final state, one should note that since the transfer-ionization process of the H^- ion is essentially a four-body problem, it is rather a formidable task to deal with an accurate final-state wave function. Thus, for feasibility, one has to resort to some approximations in constructing the final-state wave function Ψ_f^-.

In the present correlated scattering model, the incident e^+ is assumed to interact only with one of the bound electrons to be captured to form a Ps atom in the final state while the ionization of the other bound electron is supposed to be caused by the electron-electron correlation effect. The final-state wave function Ψ_f^- in the present prescription is chosen as

$$\begin{aligned}\Psi_f^-(\vec{r}_1,\vec{r}_2,\vec{r}_3) = &\exp(i\vec{k}_f\cdot\vec{R})\exp(-\lambda_f|\vec{r}_1-\vec{r}_2|)\\ &\times(2\pi)^{-3/2}M_2M_3M_{23}\exp(i\vec{k}_3\cdot\vec{r}_3)\\ &\times{}_1F_1(i\alpha_3,1;-i(k_3r_3+\vec{k}_3\cdot\vec{r}_3))\\ &\times{}_1F_1(i\alpha_2,1;-i(k_2r_2+\vec{k}_2\cdot\vec{r}_2))\\ &\times{}_1F_1(i\alpha_{23},1;-i(k_{23}r_{23}+\vec{k}_{23}\cdot\vec{r}_{23}));\end{aligned} \tag{8}$$

where $\alpha_2=-Z_t/k_2$, $\alpha_3=-Z_t/k_3$, $\alpha_{23}=1/2k_{23}$, $|\vec{k}_2|=|\vec{k}_f/2|$, $\vec{k}_{23}=(\vec{k}_2-\vec{k}_3)/2$, $\vec{R}=(\vec{r}_1+\vec{r}_2)/2$, and $M_j=\exp(\pi\alpha_j/2)\Gamma(1-i\alpha_j)$, with $j=2$, 3, or 23; λ_f is the bound-state parameter for the ground-state Ps atom $(=0.5)$.

The construction of the present final-state wave function takes account of the fact that the ejected electron (r_2) first attains a continuum state of its parent nucleus (H^- ion) and then by virtue of the $1/r_{12}$ interaction is finally captured by the incident positron to form the positronium atom (Ps) in its ground state. In the present prescription, the electron-electron correlation effect, which mainly governs the simultaneous two-electron transition, has been taken into account in both the initial and the final channels. The Ps atom could also be formed in the excited state (e.g., $2s$, $2p$), though the probability of such a process is expected to be much lower. However, the present work concentrates only on the formation of a ground-state Ps atom.

The excess energy $[E_i-E_{th}$ (threshold energy of TI)] in this transfer-ionization process is shared by two outgoing particles e^- and Ps. In the TI process the energy and momentum exchange occurs between the projectile, the electron to be captured, as well as the other bound electron that is ionized. Thus, the energy conservation relation for the process concerned is given by

$$\frac{k_i^2}{2}+\epsilon_{H^-}=\frac{k_f^2}{2\mu_f}+\frac{k_3^2}{2}+\epsilon_{Ps}, \tag{9}$$

where μ_f is the reduced mass in the final channel. $\vec{k}_i$, $\vec{k}_3$, and $\vec{k}_f$ are the respective wave vectors of the incident positron, ejected electron, and the scattered Ps atom; ϵ_{H^-} and ϵ_{Ps} are the binding energies of the ground-state negative hydrogen ion and the Ps atom, respectively. The transition amplitude T_{if} in Eq. (2) is finally reduced [13,14] to a three-dimensional integral which has been evaluated numerically.

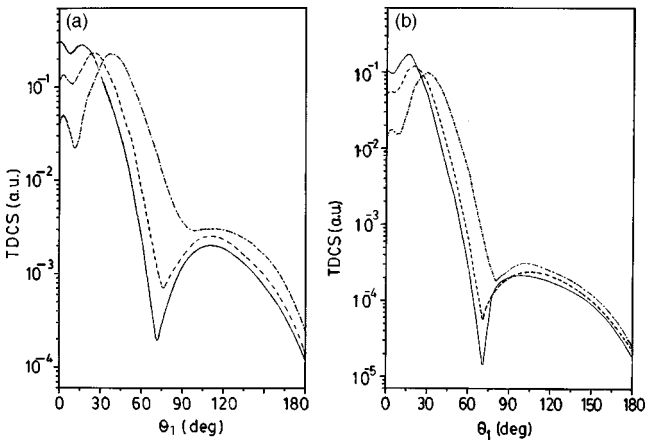

FIG. 1. (a) Angular distributions of the Ps formation in the transfer-ionization (TI) process against the Ps scattering angle θ_1 in atomic units (a.u.) for different ejected energies E_b. Incident e^+ energy $E_i=75$ eV; ejected angle $\theta_2=45°$, azimuthal angles are $\phi_1=0°$, and $\phi_2=180°$. Solid curve, $E_b=5$ eV; and dashed curve, $E_b=10$ eV; dash dotted curve, $E_b=20$ eV. (b) Same as (a) but for a higher incident energy, $E_i=100$ eV.

Finally, the fully (triple) differential cross section (TDCS) for this TI process is given by

$$\frac{d^3\sigma}{dE_2d\Omega_1d\Omega_2}=\frac{k_fk_3}{\mu_fk_i}|T_{if}|^2. \tag{10}$$

III. RESULTS AND DISCUSSION

The TDCS for the simultaneous transfer and ionization process (TI) have been studied in a positron–H^- ion collision in which the transferred electron forms a Ps atom in its ground state with the incident positron, while the other electron is ionized in a single collision. Both the dynamics of the Ps atom and the ejected electron have been studied. The threshold energy for the pure single transfer process of the e^+-H^- ion system is determined by $E_{th}(T)=E_{ion}(H^-(1s))-E_{ion}(Ps(1s))=0.75-6.8=-6.05$ eV, while the threshold energy for the TI process is given by $E_{th}TI=-6.05+13.6=7.55$ eV, since the second-ionization energy of H^- is 13.6 eV.

Figures 1(a) and 1(b) display the angular distributions of the Ps formation versus the Ps scattering angle θ_1 for two fixed incident energies [$E_i=75$ eV in Fig. 1(a) and $E_i=100$ eV in Fig. 1(b)], each with three different ejected energies (e.g., $E_b=5$, 10, 20 eV), keeping the ejected angle fixed at $\theta_2=45°$. The azimuthal angles are fixed at $\phi_1=0°$ and $\phi_2=180°$ in all the cases for the study of Ps formation.

The most salient feature noted in all the Ps distribution curves of Figs. 1(a) and 1(b) is the occurrence of a double peak, one at a smaller angle ($\approx 15°-40°$) and the other at a larger angle around ($\approx 120°$), depending on the incident as well as on the ejection energies. An additional secondary humplike structure is also noted in all the curves [particularly in Fig. 1(a)] in the extreme forward direction. In the TI pro-

cess, the excess energy is shared by the two outgoing particles, the ionized electron and the Ps atom, in unknown proportions. Thus for a fixed incident energy E_i, the lower energy of the ejected electron corresponds to a higher value of the outgoing Ps energy and vice versa. The behavior of Figs. 1(a) and 1(b) can easily be explained in view of the above fact, e.g., for a given incident energy, with higher Ps energy (i.e., lower ejection energy), the Ps distribution is more and more favored in the forward direction than in the backward one, while for the reverse case i.e., with lower Ps energy (i.e., higher ejection energy) the Ps distribution is more strongly peaked in the backward direction. This feature is quite expected physically. Comparing Figs. 1(a) and 1(b), it is also noted that the forward secondary humplike structure diminishes with increasing incident energy. Figures 1(a) and 1(b) also reveal an important feature that for a fixed E_i, the signature of the double peak in the Ps distribution becomes more prominent for lower ejection energy E_b.

Since in the present prescription, the TI process is assumed to arise due to the correlated e^+-e-e scattering, the double-peak (or shoulderlike) structures occurring in the Ps distributions of Fig. 1 may be attributed to the Thomas double-scattering (p-e-e) mechanism [11] predicted for charge-transfer or transfer-ionization process in the case of high velocity heavy-particle projectiles. For heavy-particle impact, such correlated projectile-electron-electron scattering mechanism leading to TI is responsible for the narrow peak at a critical angle ≈ 0.3 mrad observed [4] in the angular (scattering angle) dependence of the He^{++} fraction from single-electron-capture reactions in a $H^+ + He$ collision at high incident energies ($\approx$200–500 keV). The signature of the Thomas peak was also observed [1] in the absolute energy and angular differential cross sections for electron emission at high incident energies in the same TI process and the peak was similarly attributed [1] to the correlated H^+-e-e scattering process.

Figure 2(a) demonstrates the variation of the Ps angular distributions in the TI process with respect to the incident energy in the range $E_i = 40$–150 eV, while the ejected electron energy E_b and the ejected angle θ_2 are kept fixed at $E_b = 10$ eV and $\theta_2 = 45°$, respectively, keeping other parameters same as in Fig. 1. The double-peak or shoulderlike structures are also noted in all the curves in Fig. 2(a). An important feature is revealed in Fig. 2(a), e.g., the signature of the Thomas peak becomes more and more prominent with increasing incident energy corroborating the experimental findings for heavy-particle impact [1,2]. It is also noted from Fig. 2(a), that the positions of the dip and peak are quite dependent on the incident energy; the higher the incident energy, the lower is the value of the Ps scattering angle θ_1 at which the corresponding dip or peak occurs.

In order to have some idea about the effect of the final-state e-e correlation, we have plotted in Fig. 2(b) similar angular distributions θ_1 of the Ps as in Fig. 2(a) but neglecting the final-state correlation term [i.e., by setting $\alpha_{23} = 0$ and $M_{23} = 1$ in Eq. (8)]. As may be noted from Fig. 2(b), the θ_1 curves are unable to exhibit the double-peak structure noted in Fig. 2(a), indicating the fact that the final-state e-e correlation is mainly responsible for the occurrence of the double peak.

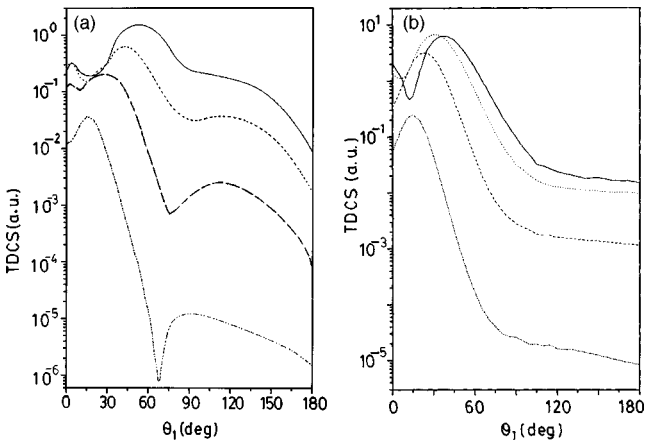

FIG. 2. (a) Same angular distributions as in Fig. 1 for different incident positron energies E_i with fixed ejection angle $\theta_2 = 45°$ and fixed ejected energy $E_b = 10$ eV. Other parameters are same as in Fig. 1. Solid curve, $E_i = 40$ eV; small dashed curve, $E_i = 50$ eV; long dashed curve, $E_i = 75$ eV; dashed double dot curve, $E_i = 150$ eV. (b) Same angular distribution as in (a) but without final-state correlation. Solid curve, $E_i = 40$ eV; small dashed curve, $E_i = 50$ eV; long dashed curve, $E_i = 75$ eV; and dashed double dot curve, $E_i = 150$ eV.

Figures 3(a) and 3(b) display the variation of the Ps distributions with respect to the ejection angle θ_2 (e.g., $\theta_2 = 5°, 45°, 90°$) for two sets of dynamics; $E_i = 75$ eV, $E_b = 5$ eV [Fig. 3(a)] and $E_i = 150$ eV, $E_b = 10$ eV [Fig. 3(b)]. As is evident from Figs. 3(a) and 3(b), the qualitative behavior of the curves for the same ejection angle θ_2 is more or less similar though the cross section is higher for lower incident energy, as is expected. The signature of the so-called Thomas double peak (or shoulder type) structures arising due to the correlated e^+-e-e scattering mechanism is also quite distinct in the Ps distribution of both Figs. 3(a) and 3(b) at

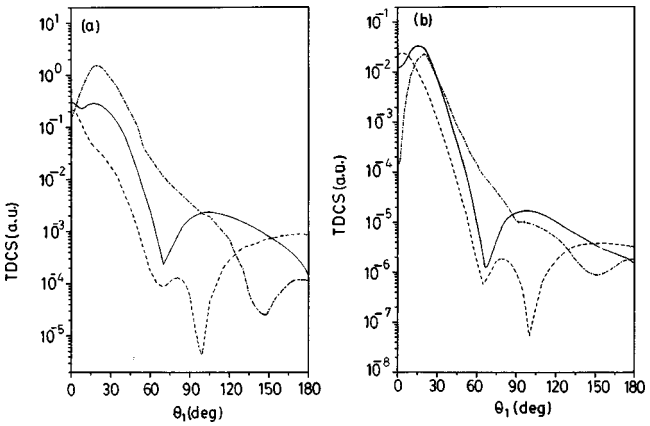

FIG. 3. (a) Same angular distributions as in Fig. 1 for different ejection angles θ_2 with fixed incident energy $E_i = 75$ eV and fixed ejected energy $E_b = 5$ eV. Other parameters are same as in Fig. 1. Solid curve, $\theta_2 = 45°$; dashed curve, $\theta_2 = 5°$; and dash dotted curve, $\theta_2 = 90°$. (b) Same as (a) but for a higher incident energy $E_i = 150$ eV and ejected energy $E_b = 10$ eV.

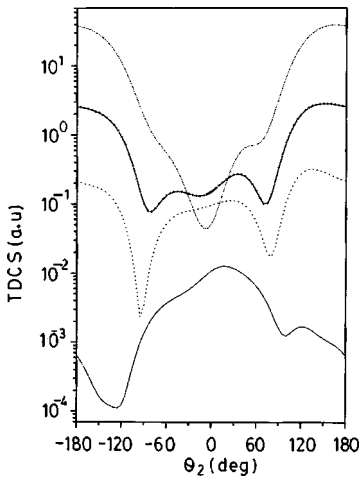

FIG. 4. Angular distributions of the ejected electron in the TI against ejection angle θ_2 in atomic units (a.u.) for different incident positron energies E_i. The Ps scattering angle is fixed at $\theta_1=5°$ and the ejected electron energy is fixed at $E_b=5$ eV. Azimuthal angles $\phi_1=0°$ and $\phi_2=0°$ and 180°. Dashed double dot curve, $E_i=50$ eV; long dashed dot curve, $E_i=75$ eV; dotted curve, $E_i=100$ eV; and solid curve, $E_i=200$ eV.

the particular ejection angle $\theta_2=45°$. However, for other ejection angles, the Thomas peak is not so prominent in these figures. It should be mentioned in this context that the angle of occurrence of the Thomas peak noted for the light projectile e^+ is at a much higher value as compared to that found for heavy-particle projectile ($\approx$mrad), as is expected physically .

For the description of the angular (θ_2) distribution of the ejected electron (Figs. 4–7), we have adopted the conventional notation for a pure ionization $(e,2e)$ process, i.e., the so-called binary region is represented by 0°–180° region ($\phi_2=180°$) while the portion of negative angle

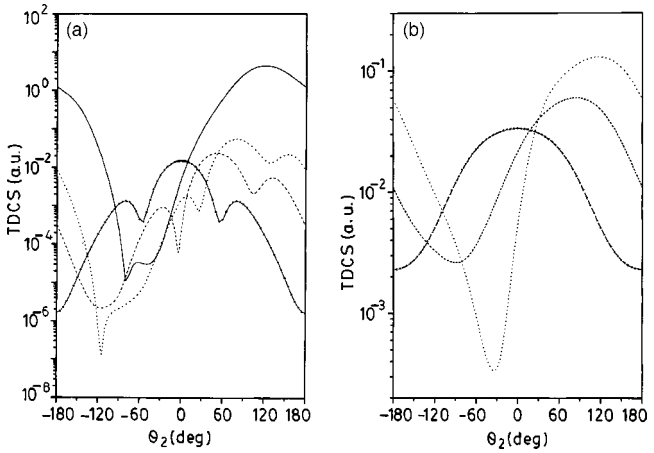

FIG. 5. (a) Same angular distributions as in Fig. 4 with incident energy 50 eV and for four different scattering angles. The ejected energy is fixed at $E_b=5$ eV. Solid curve, $\theta_1=45°$; dotted curve, $\theta_1=90°$; small dashed curve, $\theta_1=120°$; and long dashed dot curve, $\theta_1=180°$. (b) Same angular distributions as in (a) but without final-state correlation. Dotted curve, $\theta_1=90°$; small dashed curve, $\theta_1=120°$; and long dash dotted curve, $\theta_1=180°$.

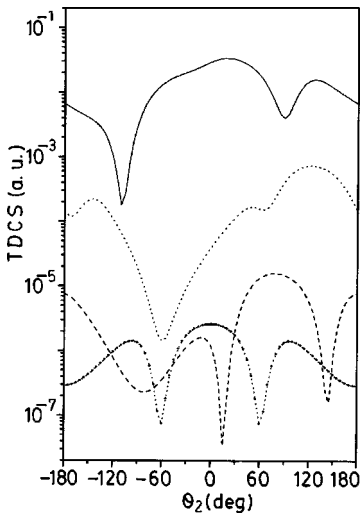

FIG. 6. Same distributions as in Fig. 5(a) but for different incident energies, i.e., $E_i=150$ eV. Solid curve, $\theta_1=5°$; dotted curve, $\theta_1=45°$; small dashed curve, $\theta_1=90°$; and dash dotted curve, $\theta_1=180°$.

0°–180°($\phi_2=0°$) represents the so-called recoil region.

Figure 4 exhibits the angular (θ_2) distributions of the ejected electron for different incident energies with a fixed ejected energy ($E_b=5$ eV) and a fixed scattering angle of the Ps ($\theta_1=5°$). A distinct qualitative difference is noted in the behavior of the present ejection angular distribution for the TI process when compared with a pure single-ionization $(e,2e)$ process [15,16], where two distinct lobes appear, one in the so-called binary region and the other in the so-called recoil region. As is evident from Fig. 4, the present θ_2 distribution for the TI process of H^- shows no such distinct peak structure in the so-called binary/recoil region. Instead, all the distributions for different E_i in Fig. 4 (except for very

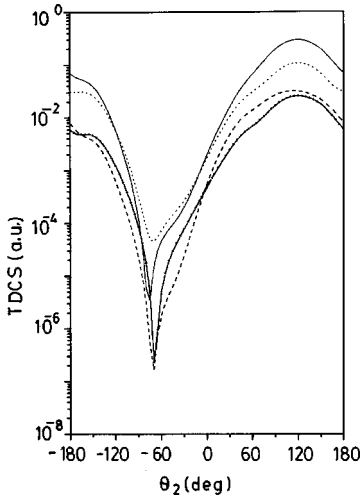

FIG. 7. Same angular distributions as in Fig. 4 with two different incident energies, $E_i=75$ eV and 100 eV and two different ejected energies. The scattering angle is fixed at $\theta_1=45°$. Solid curve, $E_i=75$, $E_b=5$ eV; dotted curve, $E_i=75$, $E_b=3$ eV; dashed curve, $E_i=100$, $E_b=10$ eV; and dash dotted curve, $E_i=100$, $E_b=5$ eV.

high incident energy, $E_i = 200$ eV) reveal that the electron is preferentially ejected in the extreme backward direction ($\pm 180°$) in both the binary and recoil regions. In fact, as may be noted from the figure, the θ_2 distribution curve for lower E_i (e.g., 50 eV) shows a central deep minimum at around $\approx 0°$ and two maxima at $\theta_2 = \pm 180°$. Such large angle ejection is quite expected physically for lower incident energy. With increasing E_i (beyond 50 eV in Fig. 4), some humplike structures start appearing in the binary and recoil regions such that finally the central minimum at $E_i = 50$ eV is replaced by a central broad maximum at $E_i = 200$ eV. This behavior could probably be explained as follows. At lower incident energy, the Ps formation is more important than the ejection while at higher E_i, the ejection dominates and hence its distribution more or less follows a single-ionization $(e,2e)$ process, although instead of the SI binary and recoil peaks, the present ejection distribution shows a broad maximum only in the binary region (vide Fig. 4, 200-eV curve) indicating that the ejection is almost binary (i.e., recoilless). However, it should be pointed out here that in the present model, the ionization of the second target electron is mainly caused by the electron-electron correlation effect instead of the projectile-electron interaction as in the case of pure SI process.

Figure 4 also indicates that the magnitude of the ejection distribution governed by the maximum intensity of the curve decreases with increasing incident energy, as is expected physically. Similar feature has been noted for the Ps distribution as well (vide Fig. 2), e.g., its peak intensity is enhanced with decreasing incident energy. Since for H^- ion, the TI threshold (≈ 7.5 eV) is quite low as compared to the present incident energies, the above behavior with respect to the variation of incident energy is quite legitimate.

Figure 5(a) represents the ejection distributions θ_2 for some higher values of the scattering angle (e.g., $\theta_1 = 45°, 90°, 120°, 180°$) of the Ps for a fixed incident energy ($E_i = 50$ eV) and fixed ejected energy ($E_b = 5$ eV). Comparing Figs. 4 and 5(a) it may be noted that for the kinematics $E_i = 50$ eV and $E_b = 5$ eV, the θ_2 distributions corresponding to $\theta_1 = 5°$ (in Fig. 4) and $\theta_1 = 45°$ [in Fig. 5(a)] are more or less similar in nature (showing no signature of double peak) except that the whole structure in Fig. 5(a) is shifted towards the recoil side. However, there is a large difference in magnitude (measured by the peak values) between the two curves, being higher for lower scattering angle θ_1 (in Fig. 4), indicating that for this particular kinematics, the Ps, being of much higher energy than the ejected electron, is scattered preferentially in the forward direction. This is also manifested in all the other Ps distributions in Figs. 1–3.

For higher values of θ_1 (e.g., $\theta_1 = 90°, 120°, 180°$), the ejection distribution in Fig. 5(a) shows an interesting behavior, e.g., a double-peaked structure in the so-called binary region, some unusual feature for a pure single-ionization process. However, as mentioned above, this feature is absent for lower values of θ_1 [e.g., 5° in Fig. 4 and 45° in Fig. 5(a)]. It is also evident from Fig. 5(a) that the double peak becomes more and more marked with increasing scattering angle. Figure 5(a) further indicates that for the extreme backward scattering angle ($\theta_1 = 180°$), the θ_2 curve contains a central peak (around 0°) exactly symmetrical with respect to the two secondary peaks (one in the binary and the other in the recoil region). However, for other higher values of θ_1 but $< 180°$ (e.g., $\theta_1 = 90°, 120°$) this symmetry is destroyed. In fact for these values of θ_1, the peak structure is shifted as a whole towards the binary region and the shift is more for lower value of θ_1.

Figure 5(b) depicts similar ejection θ_2 distributions as in Fig. 5(a) but without the final-state e-e correlation [i.e., $\alpha_{23} = 0$ and $M_{23} = 1$ in Eq. (8)]. Comparing Figs. 5(a) and 5(b) one can have some measure regarding the final-state e-e correlation effect, e.g., the structures appearing in Fig. 5(a) (both in the binary and recoil regions) are completely absent in Fig. 5(b) except for the main peaks. Further, the position of the main peaks in Fig. 5(b) (without correlation) are slightly shifted towards larger angle with respect to Fig. 5(a) (with correlation).

Figure 6 exhibits some variation of the ejection (θ_2) distribution with respect to θ_1 as in Fig. 5(a), but for a higher incident energy, e.g., $E_i = 150$ eV. It may be noted from the figure that for such higher incident energy and for higher values of the scattering angle θ_1 (e.g., 45°, 90°, 180°), the present ejection distribution more or less follows the behavior of a pure SI process, having distinct lobes in the binary and recoil regions. The position and height of the peaks are strongly dependent on the scattering angle θ_1. However, for $\theta_1 = 180°$, the θ_2 distribution is again found to be symmetrical with respect to the central peak (around 0°), as noted in Fig. 5(a). The appearance of a double-peak structure in the binary region for higher values of θ_1 is also noted in Fig. 6 [as in Fig. 5(a)].

Figure 7 again demonstrates some θ_2 distributions for two fixed incident energies ($E_i = 75$, 100 eV), each with two values of ejected energies E_b. The scattering angle θ_1 is however kept fixed at 45° in each case. The salient feature to be noted from Fig. 7 is that the maximum of the θ_2 distribution enhances with increasing E_b (both in the binary and recoil regions), an unusual behavior for a single-ionization process where the magnitude of the TDCS (governed by the binary and recoil peak intensities) usually increases with decreasing E_b. Further, since Fig. 7 involves distributions corresponding to a lower value of the Ps scattering angle ($\theta_1 = 45°$), no distinct peak structure is found as discussed earlier in connection with Figs. 5(a) and 6.

In Fig. 8 we have plotted the fully differential cross sections (TDCS) for the present TI process as a function of the ejected energy E_b, for two incident energies, e.g., $E_i = 75$ eV and 100 eV. The angle of ejection (θ_2) is chosen to be identical with the scattering angle of the Ps (θ_1), the angle being fixed at 45° (i.e., $\theta_1 = \theta_2 = 45°$). The corresponding azimuthal angles are kept fixed at $\phi_1 = 0°$ and $\phi_2 = 180°$. Both the curves exhibit a single broad peak at $E_b = E_{max}$ and then fall off monotonically down to a certain value, say, E_{bc}, a cutoff for the TI process (not shown in the figure up to E_{bc}). An interesting feature that may be noted from Fig. 8 is the enhancement of the cross section with increasing ejected energy E_b up to $E_b = E_{max}$. This behavior

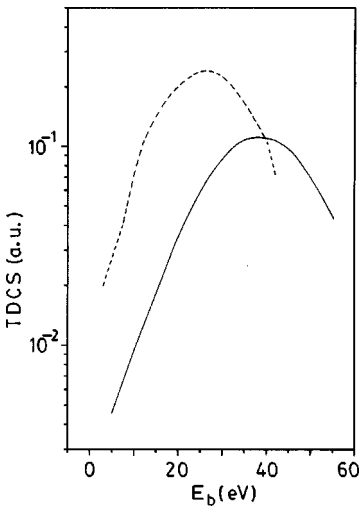

FIG. 8. Fully differential cross sections (TDCS) following the TI process against ejected energy E_b. The Ps scattering angle and the angle of ejection both are fixed at $\theta_1=\theta_2=45°$, azimuthal angles are fixed at $\phi_1=0°$ and $\phi_2=180°$, and the incident positron energy is fixed at two different values; dashed curve, $E_i=75$ eV and solid curve, $E_i=100$ eV.

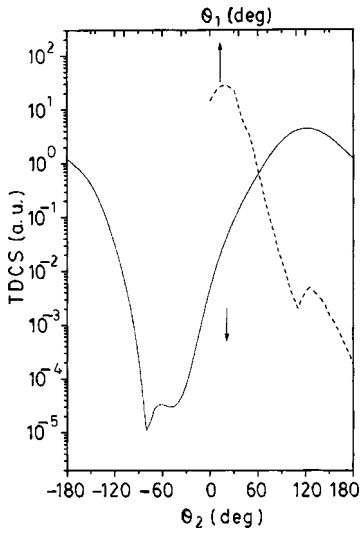

FIG. 9. The solid curve (a) represents angular distribution of the ejected electron in the TI against ejection angle θ_2 for the kinematics $E_i=50$ eV, $E_b=5$ eV, and $\theta_1=45°$. The dashed curve (b) represents the angular distribution of the Ps against scattering angle θ_1 of the kinematics $E_i=50$ eV, $E_b=5$ eV, and $\theta_2=120°$ [the angle at which the ejection curve (a) shows maximum].

of the TDCS in the lower E_b region, i.e., for $E_b<E_{max}$, is quite unusual for a pure single-ionization process (as mentioned earlier) where the TDCS decreases with increasing E_b. However, for larger E_b ($E_b>E_{max}$), the present TDCS follows the behavior of the SI process in this regard. It is also evident from Fig. 8 that the position of the peak depends on the incident energy, the higher the incident energy, the higher is the value of E_{max}. The occurrence of the cutoff at a particular value of E_b (E_{bc}) is due to the fact that for the given incident energy E_i, energy of the scattered Ps [$E_i-E_{bc}-$ threshold energy of TI] becomes zero. Obviously, E_{bc} depends on the incident energy as guided by the energy conservation relation [vide Eq. (8)]. In a similar manner, the same cutoff value can be found (for a particular E_i) in the TDCS curve as a function of the Ps energy for which the ejected energy E_b goes to zero. The exact value of E_{bc} could not be shown in Fig. 8 due to some convergence difficulty in the computation with higher values of E_b.

In the simultaneous TI process, the two processes, transfer and ionization, occur in a competitive manner, complementing each other, depending mainly on the available excess energy, i.e., for lower incident energy, the transfer process is expected to dominate while with higher incident energy, the ionization process should become more and more important. This feature could be manifested in Fig. 9 which depicts that for a lower incident energy, e.g., 50 eV, the maximum distribution of Ps is much higher than that of the ejection.

In order to show the dependence of the structures found in the present TI differential cross sections on the particular chosen model, we have demonstrated in Fig. 10 both the Ps [Fig. 10(a)] and the ejection [Fig. 10(b)] distributions for some particular kinematics using two variants of the present model along with our original results. The dashed curve represents the results without the final-state e-e correlation in Eq. (8) while retaining the initial-state (target) correlation as in Eq. (5). The dotted curve on the other hand refers to the reverse case, i.e., neglecting the initial-state correlation while retaining the final-state correlation as in Eq. (8). The solid curve in Fig. 10 represents our results from the original model [using full form of Eq. (8)].

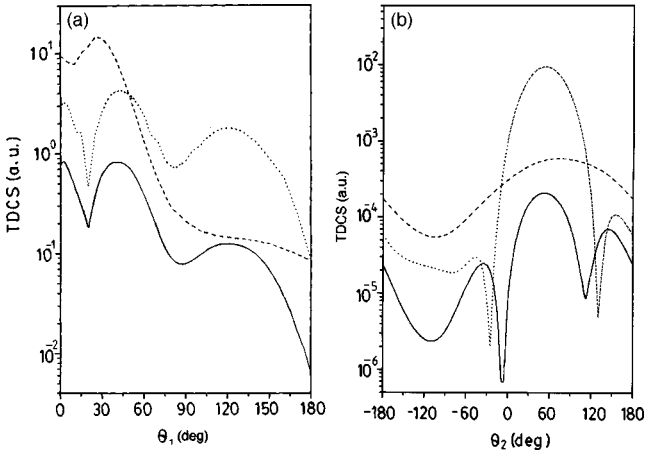

FIG. 10. (a) Angular distributions of the Ps formation in the TI process against the Ps scattering angle θ_1 using some variance of the present model for the kinematics $E_i=40$ eV, $E_b=5$ eV, and $\theta_2=45°$. The dashed curve presents the TDCS without final-state correlation [$\alpha_{23}=0$ and $M_{23}=1$ in Eq. (8)]. The dotted curve presents the TDCS without initial-state correlation [$C_0=0$ in Eq. (5)]. The solid curve represents the present result. (b) Angular distributions of the ejected electron in the TI against ejection angle θ_2 using some variance of the present model for the kinematics $E_i=100$ eV, $E_b=5$ eV, and $\theta_1=120°$. The dashed curve presents the TDCS without final-state correlation [$\alpha_{23}=0$ and $M_{23}=1$ in Eq. (8)]. The dotted curve presents the TDCS without initial-state correlation [$C_0=0$ in Eq. (5)]. The solid curve represents the present result.

Figures 10(a) and 10(b) reveal the following crucial features: (1) the double peak obtained in the solid curve (original model) is absent in the dashed curve (without final-state correlation), (2) the qualitative behavior of the dotted curve (without initial-tate correlation) and the solid curve is more or less the same, though the magnitude and the peak positions are different. It may also be noted from Fig. 10 that the results without initial-state correlation (dotted) in both figures are always higher in magnitude than those from the present original model (solid). The most important inference that can be drawn from Fig. 10 is that the final-state *e*-*e* correlation is mainly responsible for the occurrence of the double-peak structure in both the Ps and the ejection distribution curves.

IV. CONCLUSION

The present transfer-ionization process where two competing processes, e.g., formation of Ps atom and the ejection of another electron (from the H^- target) occur simultaneously is based on the correlated projectile-electron-electron scattering mechanism. The present model takes proper account of the electron-electron correlation effect in both the initial and final channels. The long-range Coulomb attraction between the incident e^+ and the negative hydrogen ion has also been incorporated in a consistent manner in the initial channel.

Both the Ps and the ejection distributions are studied and the former (Ps) is found to dominate at lower incident energies while the latter (ejection) takes over at higher incident energies, as is expected physically.

The signature of the Thomas peak as well as its becoming more and more prominent with increasing incident energy (in both the Ps and ejection distributions), predicted in the present TI fully differential cross sections, are in conformity with the experimental findings for the TI process of a noble-gas target by positron as well as by heavy-particle impact. The Thomas peak structure in the present study is also found to be quite sensitive with respect to the ejected angle/ejected energy for the Ps distribution and with respect to the scattering angle/ejected energy for the ejection distribution.

For a given incident energy, the peak intensity of the ejection distribution is found to increase with increasing ejected energy E_b, an unusual feature for a pure single-ionization process. The Ps distribution on the other hand shows the reverse behavior, e.g., its peak intensity increases with decreasing E_b.

The final-state *e*-*e* correlation (and not the initial target correlation) is responsible for the occurrence of the present double-peak structure in both the Ps and ejection distributions.

To our knowledge, for the TI process by light projectile (e^+), no measurement has yet been reported for the fully differential cross sections that contain the most detailed information about the particular process, and as such the present elaborate study (of both the Ps and the ejection distributions) is expected to provide some guidelines for the future kinematically complete experiments.

[1] J. Palinkas, R. Schuch, H. Cederquist, and O. Gustafsson, Phys. Rev. Lett. **63**, 2464 (1989).

[2] J. Palinkas, R. Schuch, H. Cederquist, and O. Gustafsson, Phys. Scr. **42**, 175 (1990).

[3] E. Horsdal-Pedersen, C.L. Cocke, and M. Stockli, Phys. Rev. Lett. **50**, 1910 (1983).

[4] Erik Horsdal, Bente Jensen, and Karsten Omann Nielsen, Phys. Rev. Lett. **57**, 1414 (1986).

[5] H. Bluhme, H. Knudsen, J.P. Merrison, and K.A. Nielsen, J. Phys. B **32**, 5237 (1999).

[6] J. Moxom, D.M. Schrader, G. Laricchia, Jun Xu, and L.D. Hulett, Phys. Rev. A **60**, 2940 (1999).

[7] T. Flake, W. Raith, and M. Weber, Phys. Rev. Lett. **75**, 3418 (1995).

[8] H. Bluhme, H. Knudsen, J.P. Merrison, and M.R. Poulsen, Phys. Rev. Lett. **81**, 73 (1998).

[9] (a) S. Geltman, Proc. Phys. Soc. London **75**, 67 (1960); (b) M.R.H. Rudge, *ibid.* **83**, 419 (1964); (c) B.E.J. Pagel, Mon. Not. R. Astron. Soc. **116**, 608 (1956).

[10] (a) B. Peart, D. S Walton, and K.T. Dolder, J. Phys. B **4**, 88 (1971); (b) T. Tanabe, I. Katayama, H. Kamegaya, K. Chida, T. Watanabe, Y. Arakaki, M. Yoshizawa, Y. Haruyama, M. Saito, T. Honma, K. Hosono, K. Hatanaka, F.J. Currell, and K. Noda, Phys. Rev. A **54**, 4069 (1996); (c) Mitio Inokuti and Yong-Ki Kim, Phys. Rev. **173**, 154 (1968); (d) P. Defrance, T.M. Kereselidze, Z.S. Machavariani, and J.V. Mebonia, J. Phys. B **32**, 2227 (1999); (e) P. Lamy, C. Dal Cappello, B. Joulakian, and C.Le. Sech, *ibid.* **27**, 3559 (1994); (f) D. Ghosh, B. Nath, and C. Sinha, *ibid.* **36**, 1479 (2003); (g) D.J. Yu, S. Rachafi, J. Jureta, and P. Defrance, *ibid.* **25**, 4593 (1992).

[11] L.H. Thomas, Proc. R. Soc. London, Ser. A **114**, 561 (1927).

[12] R.A. Bonham and D.A. Khol, J. Chem. Phys. **45**, 2471 (1966).

[13] R. Biswas and C. Sinha, J. Phys. B **28**, 1311 (1995).

[14] R. Biswas and C. Sinha, Phys. Rev. A **54**, 2944 (1996).

[15] M. Brauner, J.S. Briggs, and H. Klar, J. Phys. B **22**, 2265 (1989).

[16] R. Biswas and C. Sinha, J. Phys. B **30**, 1589 (1997).